Materials Science and Engineering B 184 (2014) 44–48

Contents lists available at ScienceDirect

Materials Science and Engineering B

journal homepage: www.elsevier.com/locate/mseb

Photosensitive and temperature-dependent *I–V* characteristics of *p*-NiO film/*n*-ZnO nanorod array heterojunction diode

Hao Long[a], Lei Ai[a], Songzhan Li[a,b], Huihui Huang[a], Xiaoming Mo[a], Haoning Wang[a], Zhao Chen[a], Yuping Liu[a], Guojia Fang[a,*]

[a] *Key Laboratory of Artificial Micro- and Nano-structures of Ministry of Education of China, Department of Electronic Science and Technology, School of Physics and Technology, Wuhan University, Wuhan, Hubei 430072, People's Republic of China*
[b] *School of Electronic and Electrical Engineering, Wuhan Textile University, Wuhan, Hubei 430073, People's Republic of China*

ARTICLE INFO

Article history:
Received 21 August 2013
Received in revised form 3 December 2013
Accepted 2 January 2014
Available online 1 February 2014

Keywords:
ZnO
NiO
Nanorod
Photosensitivity
Temperature-dependent *I–V*

ABSTRACT

A *p*-NiO film/*n*-ZnO nanorod (NR) array heterojunction was prepared by deposition of NiO film on ZnO NRs using radio-frequency reactive magnetron sputtering. The well-aligned ZnO NRs were fabricated by a simple and economic hydrothermal method on a ZnO:Al-coated glass substrate. Good morphology and crystal properties of the fabricated ZnO NRs and NiO film were confirmed by scanning electron microscopy and X-ray diffraction. The *p–n* heterojunction exhibits excellent rectifying behaviour and strong temperature-dependent current–voltage properties in the range from −50 to 80 °C. The hybrid NR heterojunction diode shows good photosensitivity under the irradiation of 365 nm ultraviolet light. These results present potential applications in future microelectronic devices based on NiO films and the one-dimensional ZnO nanomaterials.

1. Introduction

As a wide band-gap (3.37 eV) oxide semiconductor material, ZnO has been described as a good candidate for ultraviolet (UV) and blue optoelectronic applications. One-dimensional (1D) ZnO nanorods (NRs) show great potential for next-generation electronic and optoelectronic devices [1], such as photodetectors [2], solar cells [3,4], field-effect transistors [5,6], light-emitting diodes [7,8] and so on. ZnO NRs should have good UV response to enhance the performance of UV detectors due to the wide band-gap characteristics and a large surface area to volume ratio [1]. However, it is difficult to achieve *p*- and *n*-type oxide semiconductors simultaneously, which is often necessary for various device applications. For this reason, some *p*-type inorganic or organic materials such as Si [9,10], GaN [11,12], NiO [13,14], Cu_2O [15], $AgCoO_2$ [16] and $Li_{0.15}Ni_{0.85}O$ [17] were reported to fabricate the heterojunction with *n*-ZnO film or nanostructures. NiO is an inexpensive material without complex fabrication techniques and high growth temperature and is a natural *p*-type semiconductor due to the Ni vacancies with a band-gap energy of 3.7 eV, with weak absorption bands due to *d–d* transitions of $3d^8$ electron configuration in the visible region [18,19]. As *p*-type oxide semiconductor candidates, NiO [14,20] or doped NiO film [13,17,18] have been used in fabricating optoelectronic devices based on a *p–n* heterojunction with some *n*-type semiconductor materials. Numerous efforts have been made on heterostructures of *p*-NiO and *n*-ZnO [21–23]. Taking advantage of nanostructures, the heterostructure of NiO/ZnO NRs has attracted much interest of researchers [24–28]. However, there are few works on the temperature-dependent current–voltage (*I–V*) characteristics of a NiO/ZnO NR photodiode which helps understand the mechanism of the electrical transport. Here, we report fabrication and performance of a photodiode based on a *p*-NiO/*n*-ZnO NR array heterojunction. The morphology and crystal properties of the fabricated ZnO NRs and NiO film and the photosensitive and temperature-dependent *I–V* characteristics of the diode were studied.

2. Experimental

Fig. 1 illustrates the schematic diagram of the device structure. The glass substrates were ultrasonically cleaned with acetone and ethanol, respectively, for 10 min. Then, the substrates were rinsed with deionised water and blown dry with a nitrogen gun. The ZnO:Al film with a thickness of 200 nm was deposited on the glass substrates by radio-frequency (rf) reactive magnetron sputtering from a ZnO:Al target at 300 °C as the seed layer to

* Corresponding author. Tel.: +86 27 68752147; fax: +86 27 68752569.
E-mail address: gjfang@whu.edu.cn (G. Fang).

0921-5107/$ – see front matter © 2014 Elsevier B.V. All rights reserved.
http://dx.doi.org/10.1016/j.mseb.2014.01.001

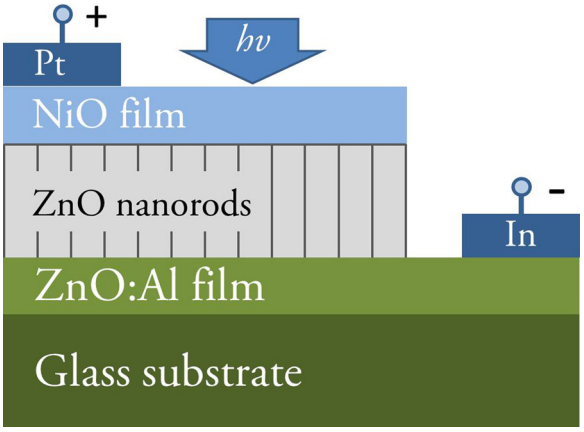

Fig. 1. Schematic diagram of the device structure.

initiate the growth of ZnO NRs. The sputtered ZnO:Al layer is electrically conductive and can serve as the n^+-contact layer. The nutrient solution for the growth of ZnO NRs via the hydrothermal method was prepared from an aqueous solution of 0.05 M zinc nitrate hexahydrate ($Zn(NO_3)_2{\cdot}6H_2O$) and 0.05 M methenamine ($C_6H_{12}N_4$). The ZnO NRs were grown by immersing the seeded substrate in a Teflon-lined autoclave up to 60% of the total volume (60 ml) at 80 °C for 7 h. The *p*-type NiO thin films with a thickness of 400 nm were subsequently deposited on top of ZnO NRs by reactive rf magnetron sputtering. According to our previous report [29], during NiO deposition, we used 99.99% pure Ni as the sputtering target, while keeping the flow rates of O_2/Ar, substrate temperature, distance between target and substrate, sputtering power, deposition time and chamber pressure at 4.0/6.0 sccm, 300 °C, 5 cm, 150 W, 90 min and 0.5 Pa, respectively. The electrical resistivities of the NiO and ZnO:Al films measured by the four-point probe method are 8.2 and 0.063 Ω cm, respectively. Pt was deposited by direct current sputtering on the NiO films as an electrode. Indium was deposited on the ZnO:Al films as the other electrode.

The morphologies and structure of the *p*-NiO/*n*-ZnO NR heterojunction were examined by field emission scanning electron microscopy (FESEM, Philips XL30, FEI, USA). The crystal structures of the ZnO NRs and NiO films were identified with X-ray diffraction (XRD, D8 Advance, Bruker AXS, USA), using X-ray diffractometer with a Ni-filtered Cu Kα radiation. The spectral transmittances of the ZnO NRs deposited on ZnO:Al/glass and NiO films deposited on glass were recorded using a ultraviolet–visible–near infrared (UV–Vis–NIR) spectrophotometer (CARY5000, Varian, USA). Current–voltage characteristics of the resultant *p*-NiO/*n*-ZnO NR heterojunction were measured using a semiconductor parameter analyzer (4200-SCS, Keithley, USA).

3. Results and discussion

Fig. 2 shows the SEM image of the ZnO NRs before and after the deposition of NiO film. As illustrated in Fig. 2(a), high-density and well-aligned ZnO NRs were grown on ZnO:Al glass templates. The inset of Fig. 2(a) shows a cross-sectional image of the as-deposited ZnO NRs. It is found that the ZnO NRs were grown vertically on the ZnO:Al/glass substrates and the average length and diameter were around 1.0 μm and 100–200 nm, respectively. The ends of the ZnO NRs are smooth and they can be easily covered by NiO thin film. Fig. 2(b) shows the cross-sectional SEM image of the ZnO NRs covered by NiO. It can be observed that the NiO film with a thickness of 400 nm was deposited on top of each individual ZnO NR and provides contacts to each ZnO NR.

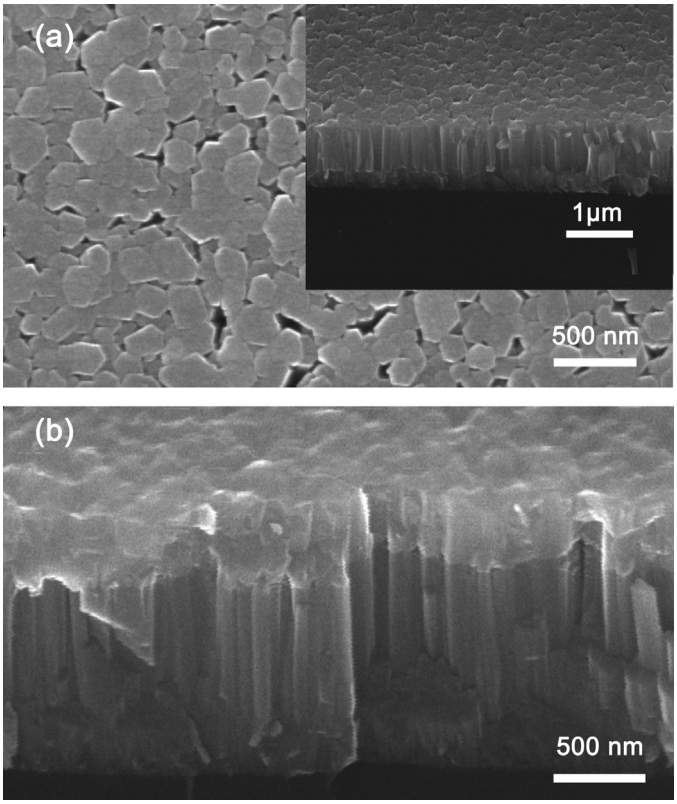

Fig. 2. (a) Top view SEM image of the as-prepared ZnO NRs, and the inset shows a cross-sectional SEM image of the as-prepared ZnO NRs. (b) Cross-sectional SEM image of the NiO deposited on ZnO NRs.

Fig. 3(a) shows the XRD spectrum of the NiO film/ZnO NRs on the ZnO:Al/glass substrate. It shows a strong (002) peak at 34.4°, indicating that the NRs were oriented preferably along the *c*-axis direction to the substrate. This is consistent with the result of the

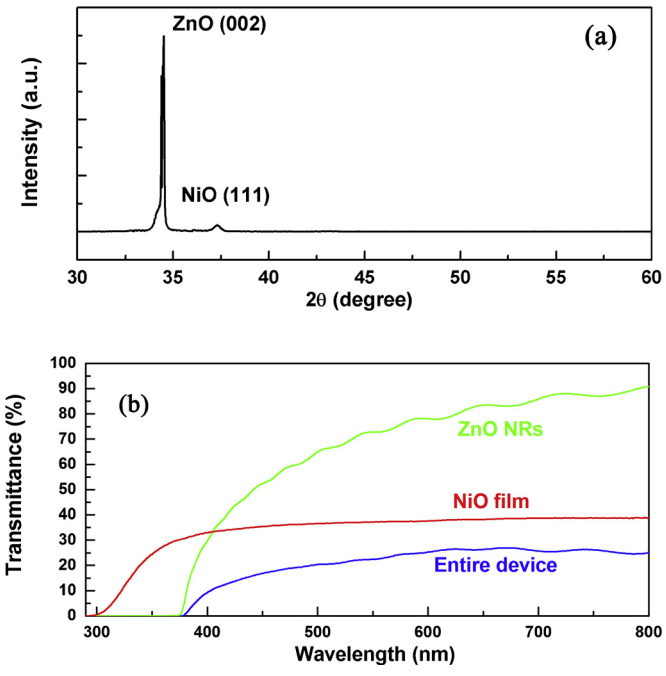

Fig. 3. (a) XRD spectrum of the NiO film deposited on ZnO NRs with a substrate of ZnO:Al/glass. (b) The transmittance spectra of the ZnO NRs, NiO thin film and the entire heterojunction diode device.

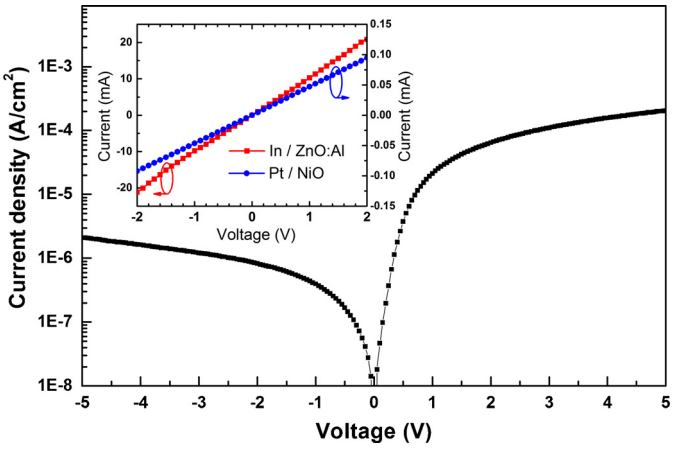

Fig. 4. *I–V* characteristics of the *p*-NiO/*n*-ZnO NRs heterojunction device at RT in logarithmic scale. The inset shows the *I–V* curves of the In/ZnO:Al and the Pt/NiO contacts, respectively.

SEM image. The ZnO single-crystal NRs were grown vertically on the ZnO:Al/glass substrate with good crystal structure. A weak peak of NiO (1 1 1) at 37.3° is also observed, which illustrates that the NiO film deposited on ZnO NR arrays has good crystal property with a NaCl-type crystal structure [29].

Fig. 3(b) shows the transmittance of the ZnO NRs, NiO film and the entire heterojunction diode device. The low transmittance of NiO films is about 35% in the range of 400–800 nm and it was decreased to 10% at 323 nm. As it was reported, the NiO thin film is semi-transparent due to the Ni^{3+} ions of Ni_2O_3, which are produced as colour centres in NiO films [30]. The low transmittance of the NiO film may be caused by the high concentration of Ni^{3+} ions. The fundamental absorption edge of the NiO thin film is located at about 330 nm, which is corresponding to the band gap of 3.7 eV. The transmittance of the entire device composed of NiO film, ZnO NRs and ZnO:Al/glass has an average transmittance of over 22% in the visible region. The absorption edge of the entire device is located at about 380 nm, which is corresponding to the band gap of 3.37 eV of ZnO.

The *I–V* characteristics of the *p*-NiO/*n*-ZnO NR heterojunction measured in the dark at room temperature (RT) are illustrated in Fig. 4, which demonstrates good rectifying property. Ohmic contacts were achieved for both electrodes as shown in the inset of Fig. 4. The threshold voltage of the *p–n* heterojunction is about 0.6 V. At this point, the current starts to increase obviously as a result of the application of a positive bias voltage. The rectification ratio is about 53.3 at a bias voltage of ±1 V. The ideality factor of the junction in the dark is 2.4. According to the Sah–Noyce–Shockley theory, the ideality factor is 1.0 at a low voltage for a diffusion-limited model, and 2.0 at a higher value for a thermionic emission model [31]. It means that the carrier recombination in the depletion region dominates the carrier transport. When the applied forward bias voltage is larger than 0.6 V, electrons in ZnO NRs may transport into the NiO film, followed by efficient recombination between the positive holes in the NiO film and the injected electrons. However, due to the presence of the lattice misfit at the interface of the junction non-ideal contact, the ideality factor could be larger than 2.0.

Temperature-dependent *I–V* behaviours shown in Fig. 5(a) were measured in a wide temperature range from −50 to 80 °C in a calorstat under the dark condition. In the *p*-NiO/*n*-ZnO NR heterojunction, with increasing temperature, the threshold voltage of the *I–V* curves decreases from 0.7 to 0.3 V and the slope becomes clearly larger in the forward bias side, which means the junction resistance decreases. Under reverse voltage, the leakage current slightly decreases.

Fig. 5(b) shows the positive bias voltage dependence of the junction resistance (R_j) at various temperatures. R_j is defined as

$$R_j = \frac{dV}{dI}. \quad (1)$$

Obviously, below the threshold voltage, R_j decreases abruptly with the increase of forward bias. When the forward bias is larger than the threshold voltage, R_j maintains a nearly invariable value. It is also noted that the threshold voltage decreases almost linearly with the increase of temperature, from 0.8 V at 80 °C to 0.48 V at −50 °C, and the junction resistance also decreases with increasing temperature. Due to the Richardson effect, carriers can be driven over the energy barrier at the NiO film/ZnO NR interface by smaller applied voltage with higher temperature [32]. Therefore, with the increase of temperature, the threshold voltage decreases and the leakage current increases.

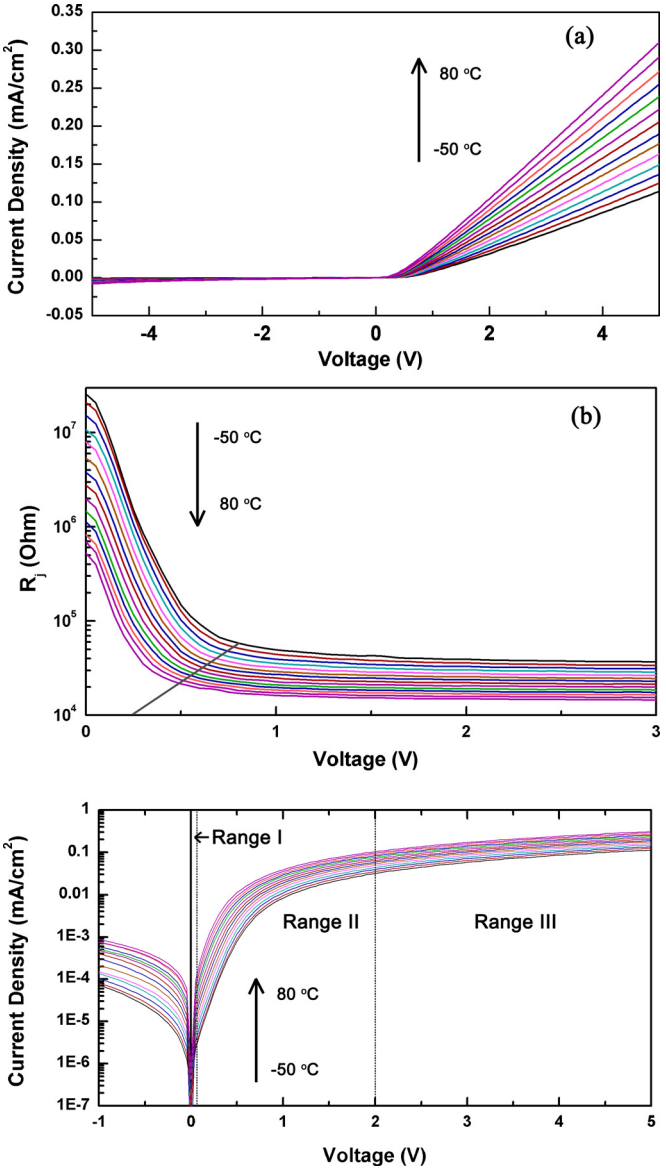

Fig. 5. (a) *I–V* characteristics of the *p*-NiO/*n*-ZnO nanorod heterojunction in a wide temperature range of −50 to 80 °C measured in dark. (b) The diode resistance $R_j = dV/dI$ as a function of the applied forward bias. The grey line delineates the threshold voltage at different temperature. (c) The temperature-dependent *I–V* curves in logarithmic scale.

The temperature-dependent I–V curves in logarithmic scale are demonstrated in Fig. 5(c). The relationship between forward current (I) and voltage (V) of a heterojunction is given approximately by

$$J(V, T) = J_0(T)\exp(AV) \quad (2)$$

where T is the temperature, A is a constant independent of the voltage and $J_0(T)$ is the reverse saturation current density. The current transport mechanism in a heterojunction can be explained by two models: (a) A is temperature dependent and can be described by

$$A = \frac{q}{nkT} \quad (3)$$

where q is the electron charge, n is the ideality factor, k is Boltzmann's constant and $n = 1.0$ for a diffusion-limited model and 2.0 for a thermionic emission model; and (b) A is independent of temperature for a tunnelling-limited model. The total current density is the sum of the currents caused by various mechanisms, but one of those is usually dominant in a certain voltage range [33].

As shown in Fig. 5(c), in the low-voltage range I of 0–0.05 V, the slopes of the forward currents on a logarithmic plot depend strongly on temperature. The relationship between forward-current density and voltage is approximately given by Eqs. (2) and (3). This behaviour is in accordance with the thermionic emission mechanism. At voltage range II (from 0.05 to 2 V), the curve departure from the ideal is due to both the heavy current injection effects and the series resistance effect. In the voltage range III (above 2 V), I–V curves are almost parallel indicating that the current depends less on temperature. It can be explained by a tunnelling model which is attributed to the recombination of electrons, tunnelling from n-type ZnO NRs into the gap states in p-type NiO, and holes tunnelling across the heterojunction barrier from p-NiO to n-ZnO NRs, where they hop between localised states through a tunnelling process. The relationship between forward current density and voltage of a heterojunction can also be given by Eq. (2), where A is a temperature-independent constant and $J_0(T)$ is a constant which shows a weak relationship with temperature.

The UV and visible photoresponsivity of the heterojunction measurement was performed using an Hg lamp with a peak at the wavelength of 365 nm under reverse bias conditions. Fig. 6(a) shows the photoresponsivity spectra of the device. From the curve, the p-NiO/n-ZnO NR device exhibits a spectral response mainly at 400 nm and the peak responsivity is about 6 mA W^{-1}. The dependence of photocurrent on operating time for the heterojunction under 365-nm illumination at the bias of −4 V is shown in the inset of Fig. 6(a). The response time of the device is about 20 s, and the recovery time (the photocurrent decreases 80%) is above 30 s. Fig. 6(b) shows the reversed I–V characteristics of the device measured in the dark and under different light intensity illumination. It can be seen that the reverse current value at a given voltage for the heterojunction under illumination is higher than that in the dark. The responsivity of this heterojunction under a reverse bias of −5 V is 2.23 mA W^{-1}. The increase of the UV-driven current under reverse bias indicates absorption and photo-carrier generation in ZnO NRs [1]. The photocurrent I_{ph} is expressed as

$$I_{ph} = Aq(\Delta n_{ph} v_n + \Delta p_{ph} v_p) \quad (4)$$

where Δn_{ph} and Δp_{ph} are the respective average electron and hole densities generated by the UV light, and v_n and v_p are the respective average velocities of electrons and holes. With the increase of reverse bias voltage, the electric field strength inside the depletion region will increase, and the electrons and holes will have higher average velocities. As a result, the photocurrent increases with the increase of reverse bias voltage. When the junction is under reverse bias, the carrier concentration in the depletion region is reduced below their equilibrium values, leading to the thermal generation

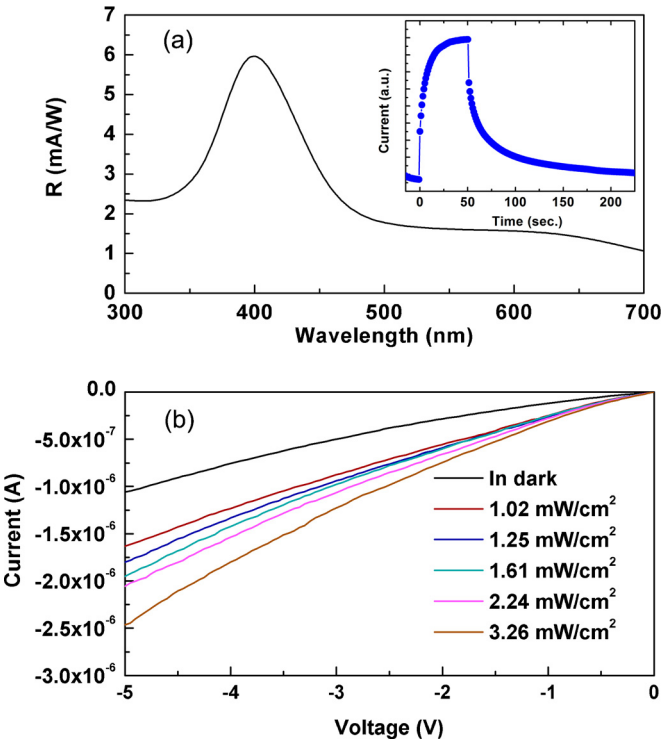

Fig. 6. (a) Photoresponsivity spectra of the p-NiO/n-ZnO NRs heterojunction photodiode. The inset shows the dependence of photocurrent on operating time for the heterojunction under 365-nm illumination at the bias of −4 V. (b) Photocurrent curves of the device towards different ultraviolet light intensity.

of electrons and holes throughout the region. The generated carriers are swept rapidly into the quasi-neutral regions by the large electric field, adding to the dark current. Therefore, as illustrated in Fig. 6(b), the dark current continually increases with increasing reverse bias voltage, but never saturates.

Compared to the previous relative reports, the efficiency of this p-NiO/n-ZnO NR heterojunction photodiode is not high. This might be affected by several factors. The NiO film deposited by rf reactive sputtering in our work exhibits a high resistance, which can be reduced by optimising the preparing condition and doping Li or other elements [34]. Material defect of the ZnO NRs and NiO film also affects the efficiency. Defect centres usually act as recombination centres of carriers in semiconductor materials. Suppression and even removal of defect centres would elongate the lifetime of carriers and then increase the photodetector response [35]. Moreover, the low transmittance of NiO reduces the light arriving at the interface of the p–n junction and ZnO NRs, and then reduces the device efficiency. So, improving the transmittance of the NiO film should enhance the performance of the device.

4. Conclusion

In summary, the p-NiO film/n-ZnO NR heterojunction diode was prepared by deposition of NiO film on as-prepared ZnO NRs. The ZnO NRs were fabricated by the hydrothermal method on the ZnO:Al/glass substrate. The SEM images show the high-density well-aligned ZnO NRs with smooth tips and the NiO deposited on ZnO NRs. The XRD pattern indicates that the ZnO is single crystalline and the NiO film is with a NaCl-type crystal structure. The transmittance results show that both the NiO films and ZnO NR arrays are semi-transparent. The heterojunction exhibits excellent rectifying behaviour and strong temperature-dependent I–V characteristics. A responsivity of 2.23 mA W^{-1} to the 365-nm UV illumination is obtained under a reverse bias of −5 V. These results may pave the

way for the application of low-cost ZnO NR solar-blind UV photodetectors.

Acknowledgements

This work was supported by the National Natural Science Foundation of China (61376013 and J1210061), the 973 Program of China (2011CB933300), the Research Program of Wuhan Science & Technology Bureau (2013010501010141), the Natural Science Foundation of Jiangsu Province (BK20131186), the Fundamental Research Funds for the Central Universities (201120202020002) and the Academic Award for Excellent Ph.D. Candidates funded by Ministry of Education of China (5052012202002).

References

[1] L. Luo, Y. Zhang, S.S. Mao, L. Lin, Sens. Actuators A 127 (2006) 201–206.
[2] S.M. Hatch, J. Briscoe, S. Dunn, Adv. Mater. 25 (2013) 867–871.
[3] E.L. Lim, C.C. Yap, M. Yahaya, M.M. Salleh, Semicond. Sci. Technol. 28 (2013) 045009.
[4] N.K. Huu, D.Y. Son, I.H. Jang, C.R. Lee, N.G. Park, ACS Appl. Mater. Interfaces 5 (2013) 1038–1043.
[5] A.N. Gruzintsev, A.N. Redkin, C. Opoku, M.N. Shkunov, Semiconductors 47 (2013) 538–542.
[6] Y.K. Park, H.S. Choi, J.H. Kim, J.H. Kim, Y.B. Hahn, Nanotechnology 22 (2011) 185310.
[7] C.H. Chao, W.H. Lin, C.H. Chen, C.H. Changjean, C.F. Lin, Semicond. Sci. Technol. 24 (2009) 105017.
[8] X.M. Mo, G.J. Fang, H. Long, S.Z. Li, H.H. Huang, H.N. Wang, Y.H. Liu, X.Q. Meng, Y.P. Zhang, C.X. Pan, J. Lumin. 137 (2013) 116–120.
[9] S. Hui, Z. Qi-Feng, W. Jin-Lei, Nanotechnology 17 (2006) 2271.
[10] J.D. Lee, C.Y. Park, H.S. Kim, J.J. Lee, Y.G. Choo, J. Phys. D: Appl. Phys. 43 (2010) 365403.
[11] Y.Q. Bie, Z.M. Liao, P.W. Wang, Y.B. Zhou, X.B. Han, Y. Ye, Q. Zhao, X.S. Wu, L. Dai, J. Xu, L.W. Sang, J.J. Deng, K. Laurent, Y. Leprince-Wang, D.P. Yu, Adv. Mater. 22 (2010) 4284.
[12] H.Z. Zhang, R.S. Shen, H.W. Liang, Y.D. Liu, Y. Liu, X.C. Xia, G.T. Du, J. Phys. D: Appl. Phys. 46 (2013) 065101.
[13] H. Ohta, M. Hirano, K. Nakahara, H. Maruta, T. Tanabe, M. Kamiya, T. Kamiya, H. Hosono, Appl. Phys. Lett. 83 (2003) 1029–1031.
[14] Y.M. Lee, H.W. Yang, C.M. Huang, J. Phys. D: Appl. Phys. 45 (2012) 225302.
[15] T.J. Hsueh, C.L. Hsu, S.J. Chang, P.W. Guo, J.H. Hsieh, I.C. Chen, Scr. Mater. 57 (2007) 53–56.
[16] R.S. Ajimsha, K.A. Vanaja, M.K. Jayaraj, P. Misra, V.K. Dixit, L.M. Kukreja, Thin Solid Films 515 (2007) 7352–7356.
[17] L. Zhuang, K.H. Wong, Appl. Phys. A 87 (2007) 787–791.
[18] H. Ohta, M. Kamiya, T. Kamiya, M. Hirano, H. Hosono, Thin Solid Films 445 (2003) 317–321.
[19] A. Fujimori, F. Minami, Phys. Rev. B 30 (1984) 957–971.
[20] K. Wang, Y. Vygranenko, A. Nathan, Thin Solid Films 515 (2007) 6981–6985.
[21] S.Y. Tsai, M.H. Hon, Y.M. Lu, Solid State Electron. 63 (2011) 37–41.
[22] M. Cavas, R.K. Gupta, A.A. Al-Ghamdi, O.A. Al-Hartomy, F. El-Tantawy, F. Yakuphanoglu, J. Sol-Gel Sci. Technol. 64 (2012) 219–223.
[23] N. Park, K. Sun, Z.L. Sun, Y. Jing, D.L. Wang, J. Mater. Chem. C 1 (2013) 7333–7338.
[24] P.Y. Yang, J.L. Wang, W.C. Tsai, S.J. Wang, J.C. Lin, I.C. Lee, C.T. Chang, H.C. Cheng, J. Nanosci. Nanotechnol. 11 (2011) 5737–5743.
[25] M.A. Abbasi, Z.H. Ibupoto, A. Khan, O. Nur, M. Willander, Mater. Lett. 108 (2013) 149–152.
[26] K.R. Lee, B.O. Jung, S.W. Cho, K. Senthil, H.K. Cho, J. Mater. Res. 28 (2013) 2605–2610.
[27] P.N. Ni, C.X. Shan, S.P. Wang, X.Y. Liu, D.Z. Shen, J. Mater. Chem. C 1 (2013) 4445–4449.
[28] R.C. Wang, M.G. Chen, Sens. Actuators B 178 (2013) 212–216.
[29] L. Ai, G.J. Fang, L.Y. Yuan, N.S. Liu, M.J. Wang, C. Li, Q. Zhang, J. Li, X.Z. Zhao, Appl. Surf. Sci. 254 (2008) 2401–2405.
[30] M. Kitao, K. Izawa, K. Urabe, T. Komatsu, S. Kuwano, S. Yamada, Jpn. J. Appl. Phys. 33 (1994) 6656.
[31] C.X. Wang, G.W. Yang, H.W. Liu, Y.H. Han, J.F. Luo, C.X. Gao, G.T. Zou, Appl. Phys. Lett. 84 (2004) 2427–2429.
[32] H. Guo, Y. Huang, K. Jin, Q. Zhou, H. Lu, L. Liu, Y. Zhou, B. Cheng, Z. Chen, Appl. Phys. Lett. 86 (2005) 123502.
[33] Y.Z. Cheng, G.J. Fang, C. Li, L.Y. Yuan, L. Ai, B. Chen, X.Z. Zhao, Z. Chen, W. Bai, C. Zhan, J. Appl. Phys. 102 (2007) 083516.
[34] C.C. Wu, C.F. Yang, Nanoscale Res. Lett. 8 (2013) 33.
[35] L.C. Yang, R.X. Wang, S.J. Xu, Z. Xing, Y.M. Fan, X.S. Shi, K. Fu, B.S. Zhang, J. Appl. Phys. 113 (2013) 084501.